BEAMFORMER DESIGN UNDER TIME-CORRELATED INTERFERENCE AND ONLINE IMPLEMENTATION: BRAIN-ACTIVITY RECONSTRUCTION FROM EEG

Takehiro Kono[1], *Masahiro Yukawa*[1,2 *], *Tomasz Piotrowski*[3,4†]

1. Department of Electronics and Electrical Engineering, Keio University, Japan
2. Center for Advanced Intelligence Project, RIKEN, Japan
3. Faculty of Physics, Astronomy and Informatics, Nicolaus Copernicus University, Grudziadzka 5/7, 87-100 Torun, Poland
4. Interdisciplinary Center for Modern Technologies, Nicolaus Copernicus University, Wilenska 4, 87-100 Torun, Poland

ABSTRACT

We present a convexly-constrained beamformer design for brain activity reconstruction from non-invasive electroencephalography (EEG) signals. An intrinsic gap between the output variance and the mean squared errors is highlighted that occurs due to the presence of interfering activities correlated with the desired activity. The key idea of the proposed beamformer is reducing this gap without amplifying the noise by imposing a quadratic constraint that bounds the total power of interference leakage together with the distortionless constraint. The proposed beamformer can be implemented efficiently by the multi-domain adaptive filtering algorithm. Numerical examples show the clear advantages of the proposed beamformer over the minimum-variance distortionless response (MVDR) and nulling beamformers.

Index Terms— Electroencephalography, inverse ploblems, relaxed zero forcing, MVDR beamformer, nulling beamformer.

1. INTRODUCTION

Electroencephalography (EEG) is the imaging modality that provides a direct measure of the brain activity by measuring the voltage with a set of sensors at various location on the scalp of the subject, and the EEG inverse problem aims to localize and reconstruct the sources of brain electrical activity from the EEG measurements. For solving this problem, the minimum-variance distortionless response (MVDR) beamformer has been used [1]. Here, we use the terminology MVDR rather than the linearly constrained minimum variance (LCMV) beamformer (which is used in [1]) since LCMV is a more general term (see below). The MVDR beamformer suppresses the interfering signals as well as the additive noise without distorting the desired signal. MVDR achieves the highest signal to interference plus noise ratio (SINR) among all linear beamformers (i.e., the same SINR as the minimum mean squared error (MMSE) beamformer) when the source signals are uncorrelated with each other. It is no longer optimal, however, when the activity of the sources are mutually correlated [2]. To overcome this issue, the nulling (zero-forcing) beamformer has been proposed in [2–4], imposing the additional nulling constraints to cancel the interfering activities generated from the other sources. Both beamformers are particular examples of the LCMV beamformer and can be implemented by efficient adaptive algorithms such as the constrained normalized least mean square (CNLMS) algorithm [5]. While the nulling beamformer outperforms MVDR when the signal-to-noise ratio (SNR) is high, it performs worse than MVDR under low SNR because of noise amplification [4]. This means that an appropriate choice of algorithm depends on the SNR condition. Signal correlation still remains a challenging issue to be addressed in the brain signal processing area. This is especially true for applications requiring online processing of beamformer output such as brain-computer interface (BCI) [6, 7] and source-space EEG neurofeedback, which is currently another hot topic in brain signal processing [8, 9]. To date, the dominant beamforming technique used in these fields has been the MVDR beamformer, see, e.g., [10–12]. Therefore, an introduction of a beamformer design which suppresses efficiently interfering activity, includes as special cases the MVDR and nulling beamformers, and is amenable to efficient adaptive implementation, should bring significant benefit to BCI and source-space EEG neurofeedback.

In this paper, we depart the world of linearity and propose a "convexly-constrained" beamformer that bounds the total power of interference leakage with the target signal kept undistorted. In the presence of correlated signals, the mean squared error (MSE) function contains a term that depends on the correlation coefficients multiplied by the filtered interfering signals. As the correlation coefficients are assumed unknown in the current study, our rough idea is to make this term vanish for avoiding the increase of MSE. Our quadratic constraint is reasonable that enforces the total interference-output-power below a prespecified threshold, because complete annihilation of the interfering signals causes noise amplification as mentioned already. The proposed beamformer resides between the MVDR and nulling beamformers in general cases, containing those beamformers as extreme cases at the two ends. Since the proposed beamformer employs the nonlinear constraint, the classical linear methods cannot be used for adaptive implementation. Fortunately, however, the constraint is convex and is also simple in a certain transform domain, the multi-domain method [13] can be applied for implementing the proposed beamformer adaptively. Numerical examples show that the proposed beamformer achieves significant gains over the whole range of SNR and that its performance is fairly close to the theoretical bound (the performance of MMSE) for high SNRs.

2. NOTATION AND EEG FORWARD MODEL

Throughout, $\mathbb{R}$ and $\mathbb{N}$ denote the sets of real numbers and nonnegative integers, respectively. Given any matrix $\boldsymbol{A}$, $\boldsymbol{A}^\top$ denotes its transpose, and $\sigma_{\max}(\boldsymbol{A})$ its largest singular value. The identity matrix is denoted by $\boldsymbol{I}$. Given real vectors $\boldsymbol{x}$, $\boldsymbol{y} \in \mathbb{R}^m$ of arbitrary dimension $m \in \mathbb{N}^* := \mathbb{N}\backslash\{0\}$, define the inner product by $\langle \boldsymbol{x}, \boldsymbol{y} \rangle := \boldsymbol{x}^\top \boldsymbol{y}$, and

*This work was supported by KAKENHI 18H01446.

†The work of the third author was supported by a grant from the Polish National Science Centre (UMO-2016/20/W/NZ4/00354): In search of the sources of brain's cognitive activity.

the induced norm by $\|\boldsymbol{x}\| := \langle \boldsymbol{x}, \boldsymbol{x}\rangle^{\frac{1}{2}}$. The expectation is denoted by $E(\cdot)$.

We now present the EEG forward model studied in this paper. We consider s dipole sources of brain activity and measurements at a specified time interval using an array of n EEG sensors. The EEG measurements at time instant $k \in \mathbb{N}$ is modeled as

$$\boldsymbol{y}(k) = \sum_{i=1}^{s} \boldsymbol{h}(\boldsymbol{\theta}_i) q_i(k) + \boldsymbol{n}(k) \in \mathbb{R}^n. \tag{1}$$

Here, $\boldsymbol{h}(\boldsymbol{\theta}_i) \in \mathbb{R}^n$ is the leadfield vector of the ith source for $\boldsymbol{\theta}_i = \{\boldsymbol{r}_i, \boldsymbol{u}_i\}$, where $\boldsymbol{r}_i$ is the source position and $\boldsymbol{u}_i$ is the orientation unit vector for the ith source, $q_i(k) \in \mathbb{R}$ the electric/magnetic dipole moments of the ith source at time instant k, and $\boldsymbol{n}(k) \in \mathbb{R}^n$ the noise vector representing background brain activity along with noise recorded at the sensor array. Without loss of generality, $q_1(k)$ is supposed to be the activity of the desired source, and $q_i(k)$ for $i = 2, 3, \cdots, s$ are the activities of interfering sources, which possess time correlations with the desired source.

All the source activities and noise are assumed zero-mean weakly-stationary stochastic processes. The source activities are supposed to change in time, but their positions and orientations are assumed known and remain the same during the measurement period. We also assume that the source activities $q_i(t)$ are mutually correlated but are uncorrelated with the noise $\boldsymbol{n}(k)$. In the present study, we assume no knowledge about the correlations; i.e., $E[q_1(k)q_i(k)]$s are unknown for $i = 2, 3, \cdots, s$.

The aim of the EEG inverse problem for the forward model (1) is to reconstruct the activity of the desired source $q_1(k)$ from the measurements $\boldsymbol{y}(k)$, given the known positions of the sources. A major approach to this problem is the beamforming, which processes the received vector by a spatial filter $\boldsymbol{w} \in \mathbb{R}^n$ as

$$\hat{q}_1(k) = \boldsymbol{w}^{\mathsf{T}} \boldsymbol{y}(k).$$

Here, $\hat{q}_1(k)$ is the estimate of the activity of the desired source $q_1(k)$.

3. THE PROPOSED BEAMFORMER DESIGN

We present the beamformer design for the inverse problem in the presence of correlated interferences and also its adaptive implementation based on the dual-domain adaptive algorithm (DDAA).

3.1. Relaxed Zero-forcing Beamformer

Under the present settings, the MSE function can be written as follows:

$$\begin{aligned} J_{\mathrm{MSE}}(\boldsymbol{w}) &:= E\left[\left(\boldsymbol{w}^{\mathsf{T}}\boldsymbol{y}(k) - q_1(k)\right)^2\right] \\ &= E[(\boldsymbol{w}^{\mathsf{T}}\boldsymbol{y}(k))^2 - 2q_1(k)\boldsymbol{w}^{\mathsf{T}}\boldsymbol{y}(k) + q_1^2(k)] \\ &= \underbrace{E[(\boldsymbol{w}^{\mathsf{T}}\boldsymbol{y}(k))^2]}_{\text{output variance}} + \underbrace{E[q_1^2(k)]}_{\text{signal power}} - 2E[q_1^2(k)]\boldsymbol{w}^{\mathsf{T}}\boldsymbol{h}(\boldsymbol{\theta}_1) \\ &\quad -2\sum_{i=2}^{s} E[q_1(k)q_i(k)]\, \boldsymbol{w}^{\mathsf{T}}\boldsymbol{h}(\boldsymbol{\theta}_i), \end{aligned} \tag{2}$$

In the absence of correlated activities, the fourth term of (2) disappears, and hence, under the distortionless constraint $\boldsymbol{w}^T\boldsymbol{h}(\theta_i) = 1$, the minimum output variance beamformer coincides with the MMSE beamformer. In the presence of correlated activities, however, those two beamformers can be significantly different due to the fourth term.

In this case, one may consider to annihilate the fourth term by imposing the nulling constraints $\boldsymbol{w}^{\mathsf{T}}\boldsymbol{h}(\boldsymbol{\theta}_i) = 0$ for all $i = 2, 3, \cdots, s$. This is actually the nulling beamformer. Unfortunately, the nulling beamformer is known to amplify the noise, performing poorly under highly noisy environments. We thus propose to bound the leakage of the interfering activities by some threshold $\epsilon \geq 0$, rather than annihilating the interfering activities completely. The proposed beamformer is formally given as follows:

$$\begin{cases} \text{minimize} \quad E[(\boldsymbol{w}^{\mathsf{T}}\boldsymbol{y}(k))^2] & (3) \\ \text{subject to} \quad \begin{cases} \boldsymbol{w}^{\mathsf{T}}\boldsymbol{h}_1 = 1 \quad (\Leftrightarrow \boldsymbol{w} \in C) \\ \|\boldsymbol{H}_I^{\mathsf{T}}\boldsymbol{w}\|^2 \leq \epsilon \quad (\Leftrightarrow \boldsymbol{H}_I^T\boldsymbol{w} \in B_\epsilon) \end{cases} & (4) \end{cases}$$

where $\boldsymbol{H}_I := [\boldsymbol{h}(\boldsymbol{\theta}_2)\ \boldsymbol{h}(\boldsymbol{\theta}_3) \cdots \boldsymbol{h}(\boldsymbol{\theta}_s)]$ is a channel matrix containing the leadfield vectors of interferences as its columns, and

$$C := \{\boldsymbol{w} \in \mathbb{R}^n \ : \boldsymbol{w}^{\mathsf{T}}\boldsymbol{h}(\boldsymbol{\theta}_1) = 1\} \tag{5}$$

$$B_\epsilon := \{\boldsymbol{s} \in \mathbb{R}^{s-1} \ : \|\boldsymbol{s}\|^2 \leq \epsilon\}. \tag{6}$$

In words, the proposed beamformer minimizes the output variance under a distortionless constraint and a bounded interference-leakage constraint. The solution to this problem is given by $\boldsymbol{w}_{\mathrm{RZF}} = \dfrac{\boldsymbol{R}_\epsilon^{-1}\boldsymbol{h}_1}{\boldsymbol{h}_1^{\mathsf{T}}\boldsymbol{R}_\epsilon^{-1}\boldsymbol{h}_1}$, where $\boldsymbol{R}_\epsilon := E[\boldsymbol{y}(k)\boldsymbol{y}(k)^{\mathsf{T}}] + \tau_\epsilon \boldsymbol{H}_I\boldsymbol{H}_I^{\mathsf{T}}$ and $\tau_\epsilon \geq 0$ is the Lagrange multiplier depending on the relaxation parameter ϵ. We refer to this bounded leakage beamformer as *relaxed zero forcing (RZF)* beamformer.

The RZF beamformer has been studied first in [14, 15] with a completely different motivation under the assumption (different from the present study) that the source signals are assumed mutually uncorrelated. Indeed, those previous studies show that the side information about the interference channel guides the update direction of adaptive beamformer towards the MMSE beamformer and accelerate the convergence speed significantly, although the MVDR beamformer is optimal in the MSE sense under the distortionless constraint in this case. The current work provides the first study of the RZF beamformer for correlated activities, revealing its considerable advantages over the conventional beamformers. For $\epsilon = 0$, the RZF beamformer reduces to the classical nulling beamformer. For ϵ sufficiently large (larger than the total interference leakage of MVDR), RZF reduces to the MVDR beamformer. The RZF beamformer is thus a generalization of the classical MVDR and nulling beamformers. Note that those beamformers solely contain linear constraints, while our beamformer involves both linear and quadratic constraints. As shown in Section 4, RZF significantly outperforms the MVDR and nulling beamformers for an appropriately chosen ϵ. The RZF beamformer can be implemented efficiently by the dual-domain adaptive algorithm [13] as described in the following.

3.2. Dual-domain Adaptive Algorithm

Given any closed convex subset K of a Euclidean space $\mathbb{R}^m$ of an arbitrary dimension m, the metric projection $P_K(\boldsymbol{x})$ of a point $\boldsymbol{x} \in \mathbb{R}^m$ onto K is defined by $P_K(\boldsymbol{x}) := \operatorname{argmin}_{\boldsymbol{y}} \|\boldsymbol{x} - \boldsymbol{y}\|$. (The projection is the nearest point of $\boldsymbol{x}$ in K.) The constraint $\boldsymbol{H}_I^{\mathsf{T}}\boldsymbol{w} \in B_\epsilon$ in (4) is not simple in the domain of $\boldsymbol{w}$, but it is simple in the transform (dual) domain under the transformation by $\boldsymbol{H}_I^{\mathsf{T}}$ (i.e., the projection $P_{B_\epsilon}(\boldsymbol{s})$ is easy to compute for any $\boldsymbol{s} \in \mathbb{R}^{s-1}$). Given an initial beamforming vector $\boldsymbol{w}_0 \in \mathbb{R}^n$, the DDAA update equation is then given as follows:

$$\boldsymbol{w}_{k+1} := \boldsymbol{w}_k + \lambda_k\mu_k\left(\alpha_k\boldsymbol{f}_k^{(1)} + (1-\alpha_k)\boldsymbol{f}_k^{(2)}\right),\ k \in \mathbb{N}, \tag{7}$$

where $\lambda_k \in (0, 2)$ is the step size, and $\alpha_k \in [0, 1]$, $\boldsymbol{f}_k^{(1)} := P_{V_k}(\boldsymbol{w}_k) - \boldsymbol{w}_k$ for $V_k := C \cap \{\boldsymbol{w} \in \mathbb{R}^n \ : \boldsymbol{w}^{\mathsf{T}}\boldsymbol{y}(k) = 0\}$, $\boldsymbol{f}_k^{(2)} :=$

$P_{B_\epsilon}\left(\frac{\boldsymbol{H}_I^\mathsf{T}\boldsymbol{w}_k}{\sigma_1(\boldsymbol{H}_I)}\right)-\frac{\boldsymbol{H}_I^\mathsf{T}\boldsymbol{w}_k}{\sigma_1(\boldsymbol{H}_I)}$, and $\mu_k := \frac{\alpha_k\left\|\boldsymbol{f}_k^{(1)}\right\|^2+(1-\alpha_k)\left\|\boldsymbol{f}_k^{(2)}\right\|^2}{\left\|\alpha_k\boldsymbol{f}_k^{(1)}+(1-\alpha_k)\boldsymbol{f}_k^{(2)}\right\|^2}$ if $\left\|\alpha_k\boldsymbol{f}_k^{(1)}+(1-\alpha_k)\boldsymbol{f}_k^{(2)}\right\|^2 \neq 0$, $\mu_k := 1$ otherwise. The vector $\boldsymbol{f}_k^{(1)}$ contributes to reducing the output variance in (3), while $\boldsymbol{f}_k^{(2)}$ contributes to reducing the violation of the quadratic constraint of (4). See [13, 15] for detailed properties of the algorithm.

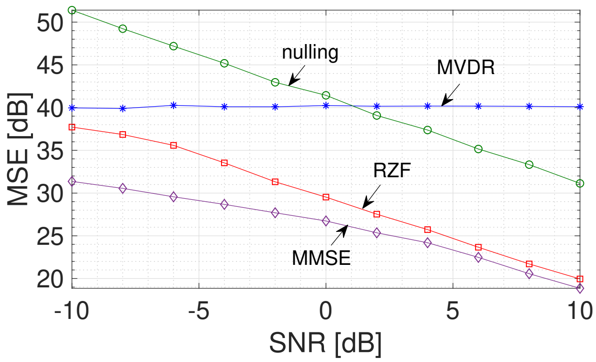

(a) $\rho = 0.3$

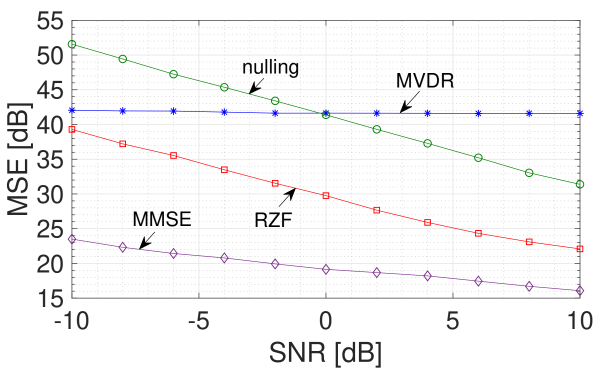

(b) $\rho = 0.9$

Fig. 1. MSE performance of the MVDR, nulling, and RZF beamformers under SIR = 0 dB in the cases of (a) low correlation and (b) high correlation.

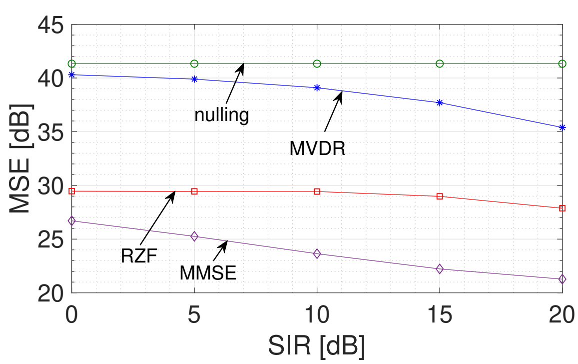

Fig. 2. MSE performance of the MVDR, nulling, and RZF beamformers under SNR = 0 dB and low correlation ($\rho = 0.3$).

4. NUMERICAL EXAMPLES

We present the numerical examples to show the efficacy of the RZF beamformer and its adaptive implementation in the presence of correlated interferences. Namely, we simulate the case of reconstructing activity of source of interest from a HydroCel Geodesic Sensor Net utilizing 128 channels as the EEG cap layout. FieldTrip (FT) toolbox [16] is used to aid generation of volume conduction model (VCM) and leadfields. We generate the activity $q_1(k)$ of the desired source by autoregressive (AR) models of order 6, and all of the coefficients for each order are set to 0.2. The number of sources is set to $s := 37$, and each interfering activity is generated as $q_i(k) = \gamma q_1(k) + \eta n_i(k)$, $\gamma > 0$, $\eta > 0$, $i = 2, 3, \cdots, s$, where $n_i(k)$ follows independently and identically distributed (i.i.d.) standard normal distribution. The strength of correlations among activities is measured by an average correlation coefficient $\rho \in [-1, 1]$ between the desired activity and the interfering ones. We consider the two cases: the low correlation case ($\rho = 0.3$ with $\gamma := 0.2$ and $\eta := 0.65$) and the high correlation case ($\rho = 0.9$ with $\gamma := 0.2$ and $\eta := 0.1$). The SNR and signal to interference ratio (SIR) are defined as the ratios of the power of desired signal projected onto sensors to the power of noise and interferences counterparts, respectively. Throughout the experiments, the power of the desired signal is fixed and those of the interference and noise are changed depending on SNR and SIR, respectively. The relaxation parameter ϵ of RZF is optimized for each SNR and SIR.

4.1. Performance of RZF Beamformer

We compare the MSE performances of the RZF, MVDR, nulling and MMSE beamformers.

Performance for different SNR: Figure 1 shows the results for SIR = 0 dB under different SNR conditions in the cases of (a) low correlation ($\rho = 0.3$) and (b) high correlation ($\rho = 0.9$). In both cases, RZF achieves significant gains compared to the MVDR and nulling beamformers. It is also seen that its performance is fairly close to the theoretical bound (that of the MMSE beamformer) in the high SNR range when $\rho = 0.3$.

Performance for different SIR: Figure 2 shows the results for SNR = 0 dB under different SIR conditions in the case of low correlation ($\rho = 0.3$). (The results are similar in the case of high correlation ($\rho = 0.9$).) One can see that the RZF beamformer achieves significant gains this time again.

Powers of noise and interference leakage: Figure 3 shows the powers of noise and interfering activities remaining in the beamformer output for SNR = SIR = 0 dB. Referring to Figure 3(b), one can see that the proposed RZF beamformer attains an excellent tradeoff; it reduces the noise leakage by allowing a slight leakage (invisible in the figure) of the interfering activities. Referring to Figure 3(a), the total leakage of RZF is even smaller than the noise leakage of MVDR. This is further analyzed below.

Sensitivity to the choice of ϵ: Figure 4(a) plots the MSE performance of RZF for each relaxation parameter ϵ for SNR = SIR = 0 dB and $\rho = 0.3$. Within the range of $1.34 < \epsilon < 3.32 \times 10^2$, the MSE of RZF is below 30 dB. This implies that RZF is reasonably insensitive to the choice of ϵ. In addition, whenever $\delta > 1.91 \times 10^{-2}$, RZF performs no worse than the MVDR and nulling beamformers. Figure 4(b) presents more precise information, plotting the power of noise/interference leakage contained in the beamformer output for different ϵ values. It is seen that both noise and interference can be suppressed simultaneously by RZF for an appropriately chosen ϵ. This supports the results of Figure 3(a) in which both noise and interference of RZF have smaller powers than the MVDR and nulling beamformers.

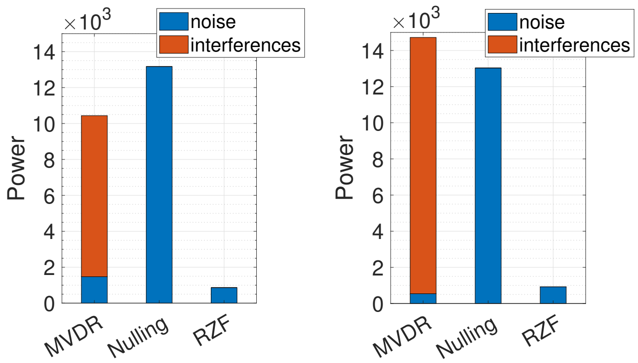

(a) $\rho = 0.3$ (b) $\rho = 0.9$

Fig. 3. Power of the noise/interference leakage for MVDR, nulling, and RZF beamformers under SNR = SIR = 0 dB in the cases of (a) low correlation and (b) high correlation.

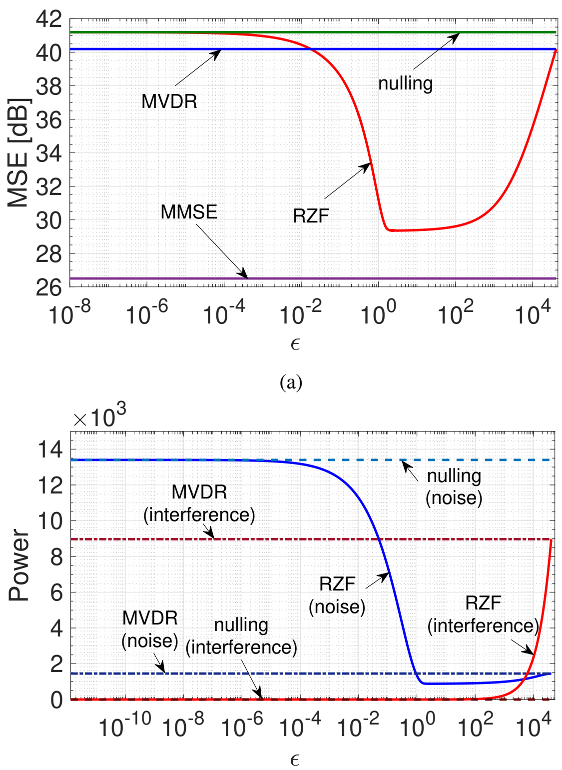

(a)

(b)

Fig. 4. (a) MSE performance of RZF beamformer for different relaxation parameters ϵ under SNR = SIR = 0 dB and low correlation ($\rho = 0.3$). (b) Powers of noise (blue) and interference (red) contained in the beamformer outputs.

4.2. Adaptive Implementation of RZF by DDAA

We compare the MSE performances of the RZF beamformer implemented by DDAA, the MVDR and nulling beamformers implemented by the CNLMS algorithm [5]. The step sizes for all online algorithms are set to $\lambda_k := 0.005$, and the weight for DDAA is set to $\alpha_k := 0.03$.

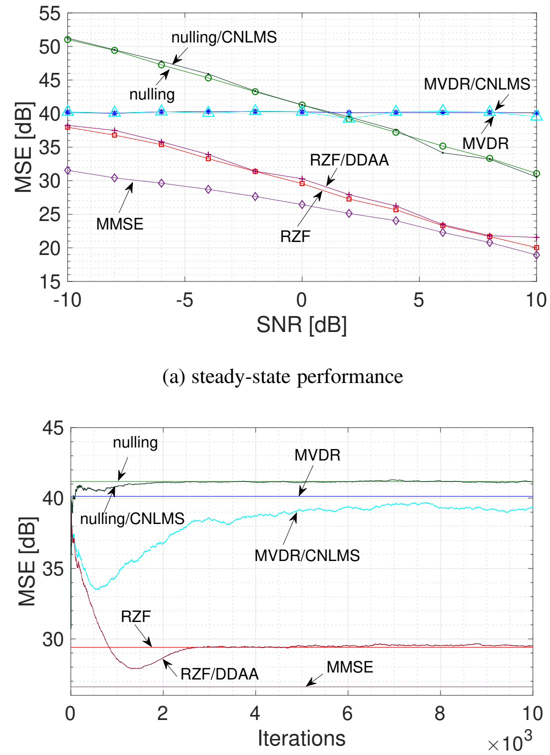

(a) steady-state performance

(b) learning curves under SNR= 0 dB

Fig. 5. MSE performance of RZF implemented with DDAA, MVDR and nulling implemented both with CNLMS under SIR = 0 dB in the case of low correlation ($\rho = 0.3$).

Figure 5(a) plots the steady-state MSE of each algorithm for SIR = 0 dB and $\rho = 0.3$ under different SNR conditions. One can see that each beamformer is successfully implemented adaptively by each adaptive algorithm. Figure 5(b) plots the learning curves for the case of SNR = 0 dB. (For visual clarity, the MSE values are averaged over the previous 3000 iterations.) It can be seen that the MSEs of the adaptive algorithms for the RZF and nulling beamformers converge reasonably fast to those of the analytical solutions, respectively. In contrast, MVDR implemented by CNLMS converges slowly due to no use of the channel information of the interfering activities.

5. CONCLUSION

We presented the RZF beamformer which minimizes the output variance under the constraints of bounded interference leakage and undistorted target signal. In the reconstruction problem of brain activity from EEG measurements, there exist correlated interfering activities which yield an intrinsic gap between MSE (unavailable) and the output variance (available). The *relaxed zero-forcing* constraint successfully reduces the gap without amplifying the noise. We also presented an adaptive implementation of the proposed RZF beamformer based on the dual-domain adaptive algorithm. Numerical examples showed that RZF significantly outperformed the MVDR and nulling beamformers.

6. REFERENCES

[1] B. D. Van Veen, W. Van Drongelen, M. Yuchtman, and A. Suzuki, "Localization of brain electrical activity via linearly constrained minimum variance spatial filtering," *IEEE Transactions on biomedical engineering*, vol. 44, no. 9, pp. 867–880, 1997.

[2] H. H. Brian, P. Dimitrios, S. L. Bressler, and R. M. Leahy, "Identifying true cortical interactions in meg using the nulling beamformer," *NeuroImage*, vol. 49, no. 4, pp. 3161–3174, 2010.

[3] S. S. Dalal, K. Sekihara, and S. S.Nagarajan, "Modified beamformers for coherent source region suppression," *IEEE Transactions on Biomedical Engineering*, vol. 53, no. 7, pp. 1357–1363, 2006.

[4] H. B. Hui and R. M. Leahy, "Linearly constrained meg beamformers for mvar modeling of cortical interactions," in *Biomedical Imaging: Nano to Macro, 2006. 3rd IEEE International Symposium on*. IEEE, 2006, pp. 237–240.

[5] J. A. Apolinário, S. Werner, P. S. Diniz, and T. I. Laakso, "Constrained normalized adaptive filters for cdma mobile communications," in *Signal Processing Conference (EUSIPCO 1998), 9th European*. IEEE, 1998, pp. 1–4.

[6] B. Wittevrongel and M. M. V. Hulle, "Hierarchical online SSVEP spelling achieved with spatiotemporal beamforming," in *2016 IEEE Statistical Signal Processing Workshop (SSP)*, June 2016.

[7] M. Mahmoodi, B. M. Abadi, H. Khajepur, and M. H. Harirchian, "A robust beamforming approach for early detection of readiness potential with application to brain-computer interface systems," in *2017 39th Annual International Conference of the IEEE Engineering in Medicine and Biology Society (EMBC)*, July 2017, pp. 2980–2983.

[8] S. Boe, A. Gionfriddo, S. Kraeutner, A. Tremblay, G. Little, and T. Bardouille, "Laterality of brain activity during motor imagery is modulated by the provision of source level neurofeedback," *NeuroImage*, vol. 101, pp. 159 – 167, 2014.

[9] S. Enriquez-Geppert, R. J. Huster, and C. S. Herrmann, "EEG-neurofeedback as a tool to modulate cognition and behavior: A review tutorial," *Frontiers in Human Neuroscience*, vol. 11, pp. 51, 2017.

[10] T. R. Mullen, C. A. E. Kothe, Y. M. Chi, A. Ojeda, T. Kerth, S. Makeig, T. Jung, and G. Cauwenberghs, "Real-time neuroimaging and cognitive monitoring using wearable dry EEG," *IEEE Transactions on Biomedical Engineering*, vol. 62, no. 11, pp. 2553–2567, Nov 2015.

[11] T. Hartmann, I. Lorenz, N. Müller, B. Langguth, and N. Weisz, "The effects of neurofeedback on oscillatory processes related to tinnitus," *Brain Topography*, vol. 27, no. 1, pp. 149–157, Jan 2014.

[12] R. van Lutterveld, S. D. Houlihan, P. Pal, M. D. Sacchet, C. McFarlane-Blake, P. R. Patel, J. S. Sullivan, A. Ossadtchi, S. Druker, C. Bauer, and J. A. Brewer, "Source-space EEG neurofeedback links subjective experience with brain activity during effortless awareness meditation," *NeuroImage*, vol. 151, pp. 117 – 127, 2017.

[13] M. Yukawa, K. Slavakis, and I. Yamada, "Multi-domain adaptive learning based on feasibility splitting and adaptive projected subgradient method," *IEICE transactions on fundamentals of electronics, communications and computer sciences*, vol. 93, no. 2, pp. 456–466, 2010.

[14] M. Yukawa, Y. Sung, and G. Lee, "Adaptive interference suppression in mimo multiple access channels based on dual-domain approach," in *Proc. ITC-CSCC*, 2011.

[15] M. Yukawa, Y. Sung, and G. Lee, "Dual-domain adaptive beamformer under linearly and quadratically constrained minimum variance," *IEEE Transactions on Signal Processing*, vol. 61, no. 11, pp. 2874–2886, 2013.

[16] R. Oostenveld, P. Fries, E. Maris, and J.-M. Schoffelen, "FieldTrip: Open source software for advanced analysis of MEG, EEG, and invasive electrophysiological data," *Computational Intelligence and Neuroscience*, p. 1, 2011.